Available online at www.sciencedirect.com
SCIENCE DIRECT®
Journal of the European Ceramic Society 25 (2005) 767–779
www.elsevier.com/locate/jeurceramsoc

A new estimation method for the intrinsic thermal conductivity of nonmetallic compounds
A case study for $MgSiN_2$, AlN and β-Si_3N_4 ceramics

R. J. Bruls[1], H. T. Hintzen, R. Metselaar*

Laboratory of Solid State and Materials Chemistry, Eindhoven University of Technology, P.O. Box 513, 5600 MB Eindhoven, The Netherlands

Received 26 February 2004; received in revised form 26 April 2004; accepted 1 May 2004
Available online 4 July 2004

Abstract

A new method for estimating the maximum achievable thermal conductivity of non-electrically conducting materials is presented. The method is based on temperature dependent thermal diffusivity data using a linear extrapolation method enabling discrimination between phonon-phonon and phonon-defect scattering. The thermal conductivities estimated in this way for $MgSiN_2$, AlN and β-Si_3N_4 ceramics at 300 K equal 28, 200 and 105 $W\,m^{-1}\,K^{-1}$, respectively in favourable agreement with the highest experimental values of 23, 266 and 106–122 $W\,m^{-1}\,K^{-1}$. This suggests the general applicability of the proposed estimation method for non-metallic compounds. It is expected that when optic phonons contribute to the heat conduction (as is the case for AlN) the intrinsic thermal conductivity at lower temperatures (e.g. 300 K) is underestimated. However, the reliability and accuracy of the presented 'easy to use' estimation method seems to be much better than several other estimation methods. Furthermore the needed input for this method can provide information about which processing parameters should be optimised to obtain the highest thermal conductivity.

Keywords: Thermal properties; Thermal conductivity; Nitrides; Substrates; Theoretical estimate; $MgSiN_2$; AlN; Si_3N_4

1. Introduction

Several ceramic materials have been investigated intensively for substrate applications[1] because of their potentially high thermal conductivity in combination with a high electrical resistivity. AlN especially has drawn a lot of attention[2–4], but recently also the nitride materials β-Si_3N_4[5–7] and $MgSiN_2$[8,9] have been considered to be potentially interesting. To estimate the intrinsic thermal conductivity one often uses Slack's equation for non-metallic materials[10]. During our work on $MgSiN_2$ we concluded that his theoretical approximation only provides a rough indication of the maximum achievable thermal conductivity, and that a more reliable and simpler estimation method would be useful.

Another (experimental) method to estimate the maximum achievable thermal conductivity is based on linear extrapolation of the measured inverse thermal conductivity (thermal resistivity)[11] versus the absolute temperature. Usually, it is assumed that the slope is determined by the lattice characteristics (intrinsic properties) and the intercept at 0 K by defects (impurities, grain boundaries, etc.)[11–13]. It will be shown that this last assumption is only partially correct, making this method not generally applicable. However, by combining some of the concepts of both approaches a new estimation method for the intrinsic thermal conductivity for non-metallic compounds was developed.

In this paper we will show that an estimation of the maximum achievable thermal conductivity of non-metallic crystals (i.e. heat transport takes place by lattice vibrations), based on temperature dependent thermal diffusivity data, gives not only more accurate information, but is also applicable over a wider temperature range. The method is applied to experimental data obtained in our own group for $MgSiN_2$[14] and to a large amount of data for AlN and β-Si_3N_4 obtained from the literature.

* Corresponding author. Tel.: +31 40 247 3122; fax: +31 40 244 5619.
E-mail address: R.Metselaar@tue.nl (R. Metselaar).
[1] Present address: ASML B.V., P.O. Box 324, 5500 AH, Veldhoven, The Netherlands.

0955-2219/$ – see front matter © 2004 Elsevier Ltd. All rights reserved.
doi:10.1016/j.jeurceramsoc.2004.05.003

2. The temperature dependence of the thermal diffusivity and conductivity

The thermal conductivity (κ [$W\,m^{-1}\,K^{-1}$]) of a material can be calculated using:[15]

$$\kappa = a\rho_m C_V \tag{1}$$

in which a [$m^2\,s^{-1}$] is the thermal diffusivity, ρ_m [$mol\,m^{-3}$] the molar density and C_V [$J\,mol^{-1}\,K^{-1}$] the heat capacity at constant volume. The density is only a weak function of temperature, so the temperature dependence of the thermal conductivity is determined by that of the thermal diffusivity and the heat capacity.

For a phonon conductor (i.e. heat transport predominantly takes place by lattice vibrations) the thermal diffusivity a equals:[15,16–18]

$$a = \frac{1}{3} v_s l_{tot} \tag{2}$$

in which v_s [$m\,s^{-1}$] is the average phonon velocity (i.e. essentially the velocity of sound) and l_{tot} [m] the total mean free path of the phonons. The average phonon velocity v_s is almost temperature independent[19], so that $a \sim l_{tot}$. If secondary phases are not taken into account then the total phonon mean free path is determined by the lattice characteristics (intrinsic properties) as well as defects and grain boundaries present in the material (extrinsic properties), and can be written as a summation of resistivities[11,20–22]:

$$\frac{1}{l_{tot}} = \frac{1}{l_{pp}} + \frac{1}{l_{pd}} + \frac{1}{l_{gb}} + \sum_x \frac{1}{l_x} \tag{3}$$

in which l_{pp} [m] is the mean free path due to thermal phonon-phonon scattering, l_{pd} [m] is the mean free path due to phonon-defect scattering (vacancies, impurities, isotopes), l_{gb} [m] is the mean free path due to phonon-grain boundary scattering and l_x [m] the mean free path due to other scattering mechanisms induced by e.g. stacking faults, dislocations, etc.

For the temperature dependence of the phonon mean free path due to thermal phonon-phonon scattering, l_{pp}, of pure crystalline materials it is known that approximately[16,23]:

$$l_{pp} = l_0 \left[\exp\left(\frac{\tilde{\theta}}{bT}\right) - 1 \right] \quad \text{with} \quad \tilde{\theta} = \frac{\theta}{n^{1/3}} \tag{4}$$

in which l_0 [m] is a pre-exponential factor, $\tilde{\theta}$ [K] a characteristic temperature (the so-called reduced Debye temperature) below which Umklapp processes start to disappear[10,24], b is a constant ≈ 2[16,17,23,25], T [K] is the absolute temperature, θ [K] is the Debye temperature and n is the number of atoms per primitive unit cell.

For most materials only the first three terms of Eq. (3) are considered to be of importance[11,21,26]. However, for the present discussion it is sufficient to assume that l_x is temperature independent. The temperature dependence of phonon-defect scattering l_{pd} has been studied by Klemens[20,27] and Ambegaokar[28]. It was shown that this term is (almost) temperature independent for low defect concentrations. The phonon-grain boundary scattering term l_{gb} is also temperature independent if the influence of the thermal expansion is neglected. So, the temperature dependence of l_{tot} is dominated by the l_{pp} term, whereas the other terms can be assumed to be temperature independent to a first approximation[11,20,29]. This implies that in general at low temperature l_{tot} is determined by temperature independent extrinsic scattering processes (at defects and grain boundaries), whereas at high temperatures it is dominated by the temperature dependent intrinsic phonon-phonon scattering process.

If the temperature is sufficiently high ($T > \tilde{\theta}/b$) we can write (including all the above mentioned phonon scattering mechanisms) for the inverse of the thermal diffusivity approximately:

$$\begin{aligned}\frac{1}{a} \sim \frac{1}{l_{tot}} &\sim \frac{A}{[\exp(\tilde{\theta}/bT) - 1]} + B \\ &= \left(\frac{bT}{\tilde{\theta}}\right) A \left[1 - \frac{1}{2}\left(\frac{\tilde{\theta}}{bT}\right) + \frac{1}{12}\left(\frac{\tilde{\theta}}{bT}\right)^2 + \cdots \right] \\ &\quad + B \approx A\left[\left(\frac{bT}{\tilde{\theta}}\right) - \frac{1}{2}\right] + B = \left(\frac{bA}{\tilde{\theta}}\right) T + \left(B - \frac{1}{2}A\right)\end{aligned} \tag{5}$$

The constant A in Eq. (5) is related to the temperature dependent phonon-phonon scattering processes (intrinsic lattice diffusivity) and B to the temperature independent phonon scattering processes (impurities, defects, grain boundaries, etc.). It is obvious that Eq. (5) shows a linear relation between a^{-1} and T:

$$a^{-1} = A'T + B' \quad \left(\text{for } T > \frac{\tilde{\theta}}{b}\right) \tag{6}$$

in which the slope A' ($= bA/\tilde{\theta}$) [$m^{-2}\,s\,K^{-1}$] is determined by the intrinsic lattice characteristics, and the intercept B' ($= B - 1/2\,A$) [$m^{-2}\,s$] by the impurities and microstructure as well as the intrinsic lattice characteristics (A). From Eq. (6) it can be concluded that for pure defect free materials ($B = 0$) a plot of the inverse of the thermal diffusivity versus the absolute temperature for measurements at $T > \tilde{\theta}/b$ extrapolated to 0 K, should result in a straight line with (negative) intercept $-1/2A$ and which intercepts the temperature axis at $T = 1/2A/A' = \tilde{\theta}/2b$.

If the temperature is sufficiently high so that the heat capacity is temperature independent ($T > \theta$[30]) then $\kappa \sim a$ ($\sim l_{tot}$) and the well known linear relation for the thermal resistivity κ^{-1} results[11–13]:

$$\kappa^{-1} = A''T + B'' \quad (\text{for } T > \theta) \tag{7}$$

This equation is often interpreted as being A'' ($\sim bA/\tilde{\theta}$) determined by the intrinsic lattice diffusivity, which is correct, and the intercept value B'' ($\sim (B - 1/2\,A)$) as being only

determined by the microstructure and impurities, which is incorrect. This results in the erroneous conclusion that for a pure defect free single crystalline material (for $T > \theta$) the thermal resistivity (κ^{-1}) versus the absolute temperature plot gives a straight line through the origin[5,12,13,31] as $B = 0$ instead of $B'' = 0$.

It is noted that at very high temperatures, where the phonon mean free path is limited by the inter-atomic distances, Eqs. (5) and (6) are no longer valid[32] because they predict a decrease of the phonon mean free path to zero. For most materials $n > 1$ so that $\tilde{\theta} < \theta$. Considering the above discussion it is clear that the linear temperature dependence for the inverse thermal diffusivity a^{-1} can be observed at much lower temperatures ($T > \tilde{\theta}/b$) than for the thermal resistivity κ^{-1} as for $T < \theta$ the heat capacity is temperature dependent. Furthermore the thermal diffusivity is directly related to the total phonon mean free path, which has to be maximised in order to optimise the thermal conductivity. So for identifying the dominant scattering mechanisms it is much more interesting to study the temperature dependence of the thermal diffusivity rather than that of the thermal conductivity.

Therefore, temperature dependent thermal diffusivity measurements when performed in a suitable temperature region ($\tilde{\theta}/b(= \theta/bn^{1/3}) \leq T$) can be a powerful tool in understanding and optimising the thermal conductivity of promising materials.

3. Experimental

For $MgSiN_2$ the thermal diffusivity a as a function of the temperature T (300–900 K) was measured on small ceramic samples (∅ 11 mm × 1 mm) cut from several large, fully dense ceramic pellets processed under different conditions (for details see Refs. 33–35) using the photo/laser flash method[36] (laser flash equipment, Compotherm Messtechnik GmbH). By carefully grinding and polishing, samples with a uniform thickness and a low roughness were obtained. Samples varying in microstructure, oxygen content and processed with and without additive were investigated (Table 1). The accuracy of the measurement was estimated to be within 5%. Some samples were coated with a thin layer of gold and/or carbon before measuring the thermal diffusivity. The thin gold layer prevents direct transmission of the laser beam and aids the energy transfer to the sample. Carbon was used to increase the absorptivity of the front surface, and the emissivity of the back surface. These additional layers reduce the measured thermal diffusivity only slightly. A gold layer is always coated with a carbon layer because the gold layer reflects the laser flash. The radiative heat losses were minimised by measuring the samples in vacuum. The molar density ρ_m and heat capacity at constant volume C_V required for calculating the thermal conductivity were obtained from our previous work (density[37] and heat capacity[37,38] assuming that $C_V = C_P$, resulting in a maximum relative error of approximately 10%[39]).

For AlN and Si_3N_4 many temperature dependent thermal diffusivity or conductivity data are reported in literature. Several AlN[4,31,40–46] and Si_3N_4[6,47–51] ceramics, with different processing conditions and thermal properties, were evaluated (see Tables 2 and 3). When necessary, the thermal diffusivity as a function of the temperature was calculated from the temperature dependence of the thermal conductivity, the density and heat capacity reported in the literature[37].

4. Results for $MgSiN_2$, AlN and β-Si_3N_4

4.1. The temperature dependence of the thermal diffusivity a

As expected, the thermal diffusivity for the $MgSiN_2$ samples processed in different ways decreases for higher

Table 1
Preparation characteristics, slope and intercept values (with R-value and intercept with the T-axis) of linearly fitted inverse thermal diffusivity (a^{-1}) vs. the absolute temperature (T), and measured room temperature (~300 K) thermal conductivity κ_{300} for several $MgSiN_2$ ceramic samples processed in different ways[33]

Sample	Densification method and reaction conditions	Additives	Oxygen content (wt.%)	Grain size (μm)	Slope A' ($m^{-2}\,s\,K^{-1}$)	Intercept B' ($m^{-2}\,s$)	R-value	Intercept T-axis (K)	κ_{300} ($W\,m^{-1}\,K^{-1}$)
RB02	Hot-pressing: 1823 K, N_2, 75 MPa, 2 h	None	3.8	–	424.6 ± 7.5	5.3 ± 4.6 × 10^3	0.9992	–	19
RB11	Hot-pressing: 1823 K, N_2, 75 MPa, 2 h	None	1.8	–	409.8 ± 8.0	27.7 ± 4.9 × 10^3	0.9990	–	16
RB13	Reaction hot-pressing: 1873 K, N_2, 75 MPa, 2 h	None	1.0	~0.5	411.8 ± 9.5	4.0 ± 5.8 × 10^3	0.9987	–	20
RB32	Reaction hot-pressing: 1873 K, N_2, 75 MPa, 2 h	4.2 wt.% Mg_3N_2	1.0	–	394.5 ± 6.6	−1.7 ± 4.0 × 10^3	0.9993	4	21
RB34	Reaction hot-pressing: 1973 K, N_2, 75 MPa, 2 h	None	1.0	~1.5	402.8 ± 4.4	−13.6 ± 2.7 × 10^3	0.9997	34	23
RB37	Reaction hot-pressing: 1873 K, N_2, 75 MPa, 2 h	6.0 wt.% Y_2O_3	–	–	437.2 ± 5.1	−19.7 ± 3.1 × 10^3	0.9997	45	22
Mean	–	–	–	–	413.5 ± 14.0	–	–	–	–

Table 2
Preparation characteristics as reported in the literature, slope and intercept values (with R-value and intercept with the T-axis) of linearly fitted inverse thermal diffusivity (a^{-1}) vs. the absolute temperature (T), and measured room temperature (∼300 K) thermal conductivity κ_{300} for several AlN ceramic samples processed in different ways

Sample	Ref.	Densification method and reaction conditions	Additives	Slope A' ($m^{-2}\,s\,K^{-1}$)	Intercept B' ($m^{-2}\,s$)	Intercept T-axis (K)	κ_{300} ($W\,m^{-1}\,K^{-1}$)
Single crystal W-201	40,61	Sublimation-recondensation: 2523 K, 95% N_2/5% H_2	None	100.0 ± 1.0	$-22.79 \pm 0.86 \times 10^3$	228	285
Shapal	41,62	Not reported		83.5 ± 1.5	$-8.08 \pm 1.10 \times 10^3$	97	141
AlN without additive	4	Hot-pressing: 2123 K, 10 min Annealing: 2123 K, 100 min	None	104.8 ± 3.0	$3.38 \pm 1.75 \times 10^3$	–	70
BP research AlN	31,62	Not reported		81.6 ± 1.0	$-14.33 \pm 0.45 \times 10^3$	176	228
Shapal SH-04	31,62	Not reported		85.6 ± 1.6	$-11.66 \pm 0.77 \times 10^3$	136	167
Shapal SH-15				91.9 ± 1.5	$-14.62 \pm 0.77 \times 10^3$	159	144
Super Shapal				84.4 ± 1.9	$-14.79 \pm 0.94 \times 10^3$	175	212
Toshiba TAN-170	31,62	Not reported		85.0 ± 1.5	$-11.69 \pm 0.69 \times 10^3$	138	170
Carborundum AlN	31,62	Not reported		82.4 ± 1.1	$-13.81 \pm 0.51 \times 10^3$	168	212
AlN	42	Pressureless sintering: 2023 K, N_2, 10 h	4 wt.% Y_2O_3	89.3 ± 9.0	$-16.11 \pm 4.21 \times 10^3$	180	208
B(N_2)	43	Pressureless sintering: 2133 K, N_2, 1 h	1 wt.% Y_2O_3	87.0 ± 1.9	$-4.72 \pm 1.05 \times 10^3$	54	119
H(N_2)			3 wt.% Y_2O_3	91.6 ± 2.4	$-13.41 \pm 1.35 \times 10^3$	146	159
G(N_2)			10 wt.% Y_2O_3	94.3 ± 1.1	$-12.74 \pm 0.58 \times 10^3$	135	148
C1	43,44	Pressureless sintering: 2098 K, N_2, 1 h	3 wt.% Y_2O_3 + 0 wt.% CaO	89.2 ± 1.0	$-10.50 \pm 0.56 \times 10^3$	118	144
I1	43		3 wt.% Y_2O_3 + 1 wt.% CaO	91.5 ± 0.5	$-9.11 \pm 0.30 \times 10^3$	100	129
B1	43,44		3 wt.% Y_2O_3 + 2 wt.% CaO	100.0 ± 1.0	$-10.97 \pm 0.52 \times 10^3$	110	124
H(N_2)	43,45	Pressureless sintering: 2133 K, N_2, 1 h	3 wt.% Y_2O_3 + 0 wt.% SiO_2	91.6 ± 2.4	$-13.41 \pm 1.35 \times 10^3$	146	159
N(N_2)	43		3 wt.% Y_2O_3 + 0.3 wt.% SiO_2	88.5 ± 0.6	$-8.19 \pm 0.32 \times 10^3$	93	129
O(N_2)	43,45		3 wt.% Y_2O_3 + 1 wt.% SiO_2	96.0 ± 1.5	$-6.62 \pm 0.83 \times 10^3$	69	106
Q(N_2)	43,45		3 wt.% Y_2O_3 + 2 wt.% SiO_2	148.9 ± 5.3	$9.10 \pm 2.93 \times 10^3$	–	46
S(N_2)	43,45		3 wt.% Y_2O_3 + 5 wt.% SiO_2	200.4 ± 11.4	$45.83 \pm 6.30 \times 10^3$	–	24

Table 3
Preparation characteristics and resulting β-fraction as reported in the literature, slope and intercept values (with *R*-value and intercept with the *T*-axis) of linearly fitted inverse thermal diffusivity (a^{-1}) vs. the absolute temperature (T), and measured room temperature (∼300 K) thermal conductivity κ_{300} for several β-Si_3N_4 and α/β-Si_3N_4 composite ceramic materials processed in different ways

Sample		Densification method and reaction conditions	Additives	β-Fraction (%)	Slope A' ($m^{-2}\,s\,K^{-1}$)	Intercept B' ($m^{-2}\,s$)	Intercept *T*-axis (K)	κ_{300} ($W\,m^{-1}\,K^{-1}$)
SN5	50	Gas-pressure sintered: 2473 K, 30 MPa (N_2), 4 h	0.5 mol% Y_2O_3 + 0.5 mol% Nd_2O_3	100	129.1 ± 2.9	$-22.84 \pm 3.14 \times 10^3$	177	122
	51	HIPped: 2673 K, 200 MPa (N_2), 2 h	3.5 wt.% Y_2O_3	100	98.9	-10.27×10^3	104	107
A	47	High pressure hot-pressing: 2173 K, 3 GPa, 1 h	None	100	125.7 ± 6.3	$42.57 \pm 4.49 \times 10^3$	–	30
B			4 wt.% MgO	100	143.6 ± 5.1	$38.46 \pm 3.51 \times 10^3$	–	29
D			4 wt.% Al_2O_3	100	251.3 ± 19.3	$106.38 \pm 13.67 \times 10^3$	–	14
C		High pressure hot-pressing: 2073 K, 3 GPa, 1 h	4 wt.% Y_2O_3	100	159.0 ± 9.5	$64.24 \pm 6.71 \times 10^3$	–	22
□	48	Capsule-HIPped: 1973 K, 60 MPa (Ar), 1 h	3 mol% Y_2O_3 + 3 mol% Al_2O_3	∼25	210.6 ± 4.3	$20.36 \pm 3.18 \times 10^3$	–	28
○			2 mol% Y_2O_3 + 4 mol% Al_2O_3	∼34	199.8 ± 6.6	$31.35 \pm 4.82 \times 10^3$	–	26
▲			4 mol% Y_2O_3 + 2 mol% Al_2O_3	∼67	146.2 ± 5.4	$48.01 \pm 3.91 \times 10^3$	–	24
■-100	48	Capsule-HIPped: 2023 K, 60 MPa (Ar), 1 h	3 mol% Y_2O_3 + 3 mol% Al_2O_3	100	143.5 ± 4.4	$38.24 \pm 4.02 \times 10^3$	–	28
■- 90		Capsule-HIPped: 1973 K, 60 MPa (Ar), 1 h	3 mol% Y_2O_3 + 3 mol% Al_2O_3	∼90	143.8 ± 6.6	$53.44 \pm 4.82 \times 10^3$	–	22
■- 34		Capsule-HIPped: 1823 K, 60 MPa (Ar), 1 h	3 mol% Y_2O_3 + 3 mol% Al_2O_3	∼34	169.2 ± 10.4	$83.86 \pm 7.56 \times 10^3$	–	16
+ 6/0	48	Capsule-HIPped: 2023 K, 60 MPa (Ar), 1 h	6 mol% Y_2O_3 + 0 mol% Al_2O_3	100	112.1 ± 1.3	$-3.77 \pm 1.20 \times 10^3$	34	73
+ 5/1			5 mol% Y_2O_3 + 1 mol% Al_2O_3	100	116.0 ± 1.2	$6.40 \pm 1.10 \times 10^3$	–	53
+ 4/2			4 mol% Y_2O_3 + 2 mol% Al_2O_3	100	127.7 ± 3.6	$26.94 \pm 3.30 \times 10^3$	–	35
+ 3/3			3 mol% Y_2O_3 + 3 mol% Al_2O_3	100	143.5 ± 4.4	$38.24 \pm 4.02 \times 10^3$	–	28
+ 2/4			2 mol% Y_2O_3 + 4 mol% Al_2O_3	100	150.9 ± 4.7	$50.57 \pm 4.34 \times 10^3$	–	23
+ 1/5			1 mol% Y_2O_3 + 5 mol% Al_2O_3	100	137.5 ± 7.4	$67.91 \pm 6.71 \times 10^3$	–	21
+ 0/6			0 mol% Y_2O_3 + 6 mol% Al_2O_3	100	146.2 ± 6.1	$92.43 \pm 5.53 \times 10^3$	–	17
Tape cast	6	Hot-pressed: 2073 K, 40 MPa, 2 h and subsequently HIPped: 2773 K, 200 MPa (N_2), 2 h	5 wt.% Y_2O_3 + 5 vol.% rod-like β-Si_3N_4 seeds	–	84.5 ± 2.1	$-8.96 \pm 1.52 \times 10^3$	106	155
					187.0 ± 4.8	$-22.29 \pm 3.10 \times 10^3$	119	70

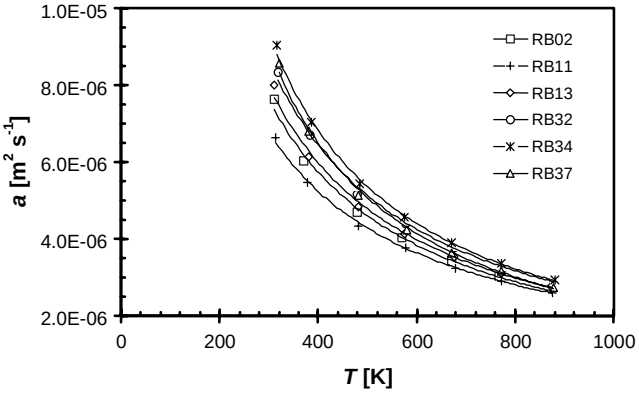

Fig. 1. The thermal diffusivity (a) plotted vs. the absolute temperature (T) for several $MgSiN_2$ samples (see Table 1).

temperatures (Fig. 1). The same is true for the AlN (Table 2) and Si_3N_4 (Table 3). For all three materials the observed thermal conductivity at 300 K varied over a relatively broad range ($MgSiN_2$: 16–23 $W\,m^{-1}\,K^{-1}$ (Table 1); AlN: 24–285 $W\,m^{-1}\,K^{-1}$ (Table 2); β-Si_3N_4: 14–122 $W\,m^{-1}\,K^{-1}$ (Table 3)), indicating large differences in impurity content and microstructure for the different samples. The difference in thermal diffusivity between the samples is less pronounced at higher temperatures (see e.g. Fig. 1) as then intrinsic phonon scattering processes are dominating the thermal diffusivity (so $A'T > B'$).

4.2. Inverse thermal diffusivity a^{-1} versus temperature T plots

As expected from theory (see Section 2), for all three compounds a linear fit of the inverse of the thermal diffusivity plotted against the absolute temperature (Figs. 2–8) resulted in a good description of the temperature dependence (typically $R > 0.99$) (Tables 1–3). The indicated uncertainties for the slope and the intercept correspond with the 95% confidence interval.

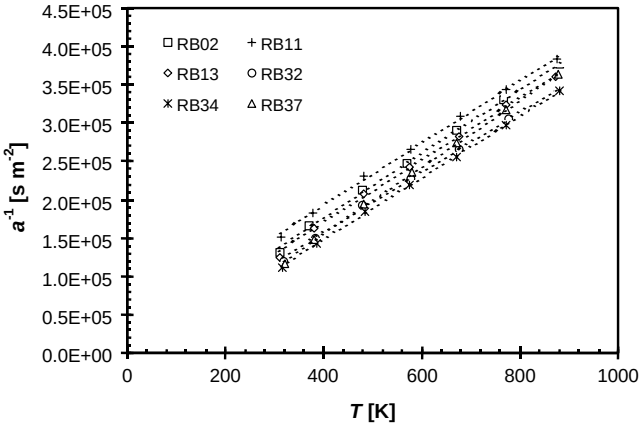

Fig. 2. The inverse thermal diffusivity (a^{-1}) vs. the absolute temperature (T) plot for $MgSiN_2$ ceramic samples processed in different ways (see Table 1).

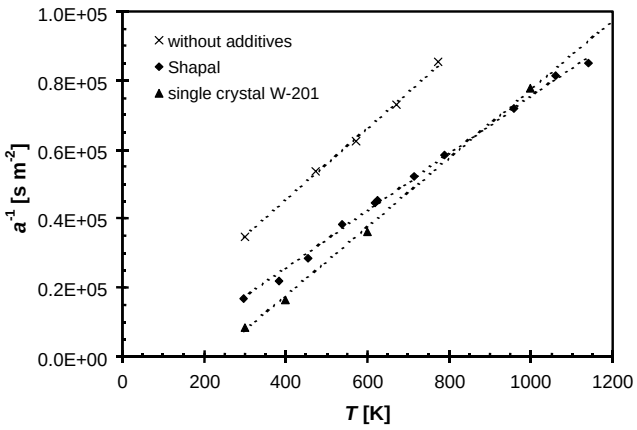

Fig. 3. The inverse thermal diffusivity (a^{-1}) vs. temperature (T) plot as obtained from literature data for AlN samples without additive (×)[4], a typical sample (◆)[41,62] and a single crystal (▲)[40] (see Table 2).

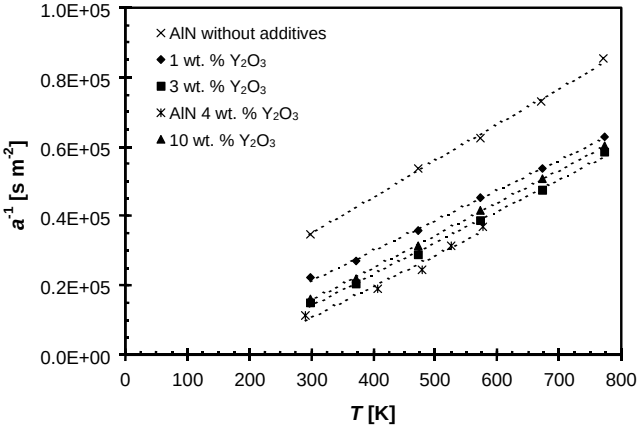

Fig. 4. The inverse thermal diffusivity (a^{-1}) vs. temperature (T) plot as obtained from literature data for AlN ceramics, processed with different amounts of Y_2O_3 as a sintering additive. Data obtained from[4] (without additives),[42] (4 wt.% Y_2O_3) and[43] (1, 3 and 10 wt.% Y_2O_3) (see Table 2).

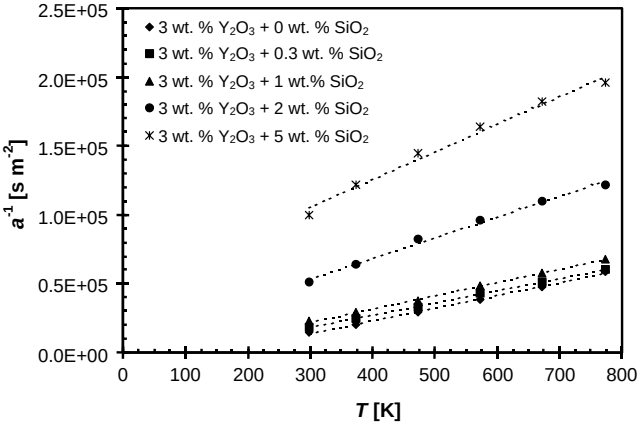

Fig. 5. The inverse thermal diffusivity (a^{-1}) vs. temperature (T) plot as obtained from literature data[43,45] for AlN ceramics, processed with 3 wt.% Y_2O_3 and different amounts of SiO_2 as sintering additives (see Table 2).

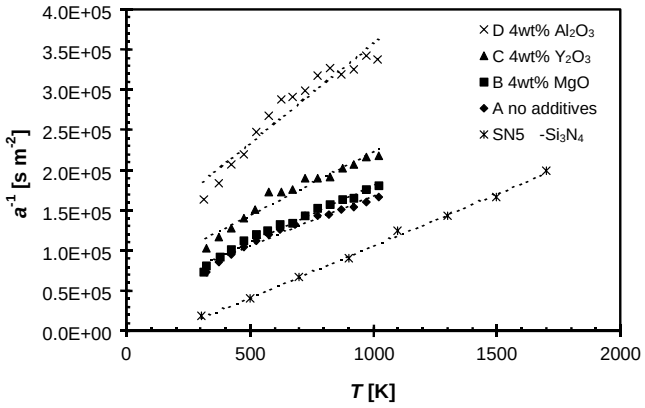

Fig. 6. The inverse thermal diffusivity (a^{-1}) vs. temperature (T) plot as obtained from literature data for β-Si_3N_4 ceramics processed in different ways. Data obtained from Ref. 47 (sample A–D) and Ref. 50 (sample SN5) (see Table 3).

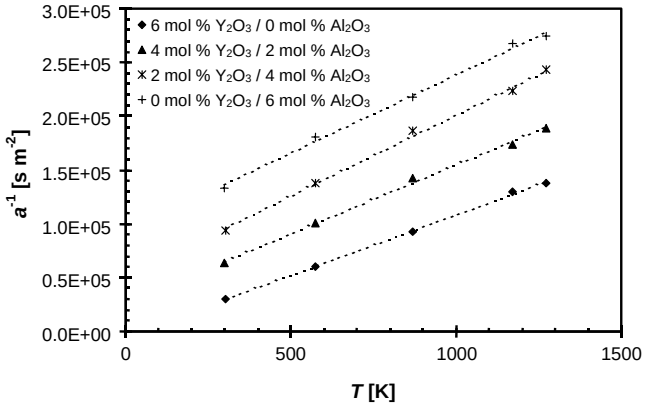

Fig. 7. The inverse thermal diffusivity (a^{-1}) vs. temperature (T) plot as obtained from literature data[48] (see Table 3) for β-Si_3N_4 ceramics using mixtures of Y_2O_3 and Al_2O_3 as sintering additives.

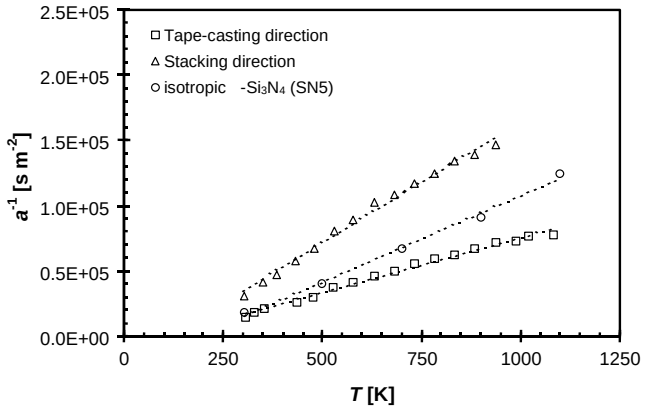

Fig. 8. The inverse thermal diffusivity (a^{-1}) vs. temperature (T) plot as obtained from literature data for β-Si_3N_4 ceramics along the casting and stacking direction as compared to an isotropic sample. Data obtained from[6] (casting and stacking direction) and[50] (sample SN5) (see Table 3).

4.2.1. $MgSiN_2$

For all $MgSiN_2$ samples about the same slope A' of 414 $\pm$ 14 $m^{-2}\,s\,K^{-1}$ is observed (Table 1 and Fig. 2) indicating that the lattice characteristics are not influenced by the processing conditions used. In contrast, the intercept B' shows a relatively large variation, as the samples differ in impurity content and grain size[33]. As expected, the samples with the highest purity and grain size have in general the lowest intercept values (Table 1).

4.2.2. AlN

The AlN ceramics processed with several different additives have a typical slope value of 80–90 $m^{-2}\,s\,K^{-1}$ (Table 2). These values are somewhat smaller than the value observed for the hot-pressed AlN sample without sintering additive (104.8 $\pm$ 3.0 $m^{-2}\,s\,K^{-1}$). This difference can be ascribed to the presence of oxygen containing secondary phases. Also for the best heat-conducting sample (single crystal W-201[40]) a somewhat larger slope is observed (100.0 $\pm$ 1.0 $m^{-2}\,s\,K^{-1}$) as compared to the typical value (Fig. 3). However, this observation may be related to the fact that this sample is a single crystal for which the thermal conductivity was determined along the c-axis.

The slope is not much influenced by the addition of small amounts of Y_2O_3 ($\leq$10 wt.%) (Fig. 4) and CaO ($\leq$2 wt.% together with 3 wt.% Y_2O_3 (Table 2)), whereas the slope changes drastically for larger amounts SiO_2 addition ($\geq$2 wt.% together with 3 wt.% Y_2O_3) (Fig. 5). From these observations it can be concluded that Y_2O_3 and CaO additions mainly influence the defect chemistry and microstructure of the AlN ceramics (phonon-defect and phonon-grain boundary scattering), whereas SiO_2 addition also results in a change of the lattice characteristics (phonon-phonon scattering). In complete agreement with this conclusion for these samples, de Baranda et al.[45] reported that for an SiO_2 addition of 2 wt.% and above, together with a 3 wt.% Y_2O_3 additive, sialon polytypoids with an AlN like structure are formed, resulting in the formation of a different lattice and thus a different slope value (Table 2 and Fig. 5).

For samples with the typical slope value of 80–90 $m^{-2}\,s\,K^{-1}$, the intercept value B' is the smallest for the (almost) defect free single crystal and largest for hot-pressed ceramics processed without additives containing many defects due to the oxygen impurities dissolved into the AlN lattice (Fig. 3 and Table 2). By suitable processing (Table 2: AlN[42]) the defect concentration in the AlN lattice is reduced resulting in a decrease of the intercept approaching the value for the (almost) defect free single crystal.

With increasing Y_2O_3 addition the intercept value B' first decreases and subsequently increases again (Table 2 and Fig. 4) in agreement with other observations[52,53] that with increasing Y_2O_3 addition the thermal conductivity first increases (till about 4–6 wt.% addition[53]) and subsequently decreases. This indicates that (as expected) Y_2O_3 is an effective sintering aid for sintering of AlN by reducing the defect concentration (Al vacancies) in the AlN lattice. For

higher dopant levels the thermal conductivity decreases because the thermal conductivity of the formed yttrium aluminates (and Y_2O_3) is much lower than that for AlN[4,52], resulting in some increase of the observed slope value too.

4.2.3. β-Si_3N_4

The lowest slope value A' for the isotropic β-Si_3N_4 samples equals 100–130 $m^{-2}\,s\,K^{-1}$ (Table 3). The slope observed for the sample with the highest thermal diffusivity (SN5) equals $129.1 \pm 2.9\,m^{-2}\,s\,K^{-1}$. The addition of MgO and Y_2O_3 has only a limited influence on the slope, whereas in contrast the addition of Al_2O_3 has a strong effect (Fig. 6). The reason for this different behaviour is that the Al_2O_3 addition can dissolve into the β-Si_3N_4 lattice resulting in the formation of a β-sialon ($Si_{6-z}Al_zO_zN_{8-z}$), whereas Y_2O_3 and MgO can only react with SiO_2 on the surface of the Si_3N_4 grains to form a separate secondary phase. The relatively large scattering in the data points for the samples A–D, especially at higher temperatures (Fig. 6), can be partially ascribed to the inaccuracy introduced when obtaining the data from a plot of Ref. 47.

For a lower β content of the α/β-Si_3N_4 composite ceramics the observed slope increases (Table 3). This observation can be explained in view of the difference between the crystal structure of the α- and β-modifications of Si_3N_4. As the α-modification is more complex than the β-modification (α-Si_3N_4: $n = 28$; β-Si_3N_4: $n = 14$) it is expected for α-Si_3N_4 to have a higher value for the slope A' (assuming that b, A, and θ are about the same for both modifications) and thus a lower intrinsic thermal conductivity than β-Si_3N_4.

A nice illustration of the influence of the type and amount of additive on the slope and intercept values can be obtained from the data of Watari et al.[48] who studied the influence of Y_2O_3 and Al_2O_3 additions totalling 6 mol% on the thermal conductivity of β-Si_3N_4 (Table 3 and Fig. 7). It can be concluded that Y_2O_3 without Al_2O_3 is an effective additive for increasing the thermal conductivity of β-Si_3N_4 because it does not dissolve in the lattice (slope $A' \approx$ constant $\approx 110\,m^{-2}\,s\,K^{-1}$) and decreases the intercept B' (<0), whereas with increasing Al_2O_3 content a sialon is formed resulting in a change of the lattice characteristics (increase of the slope A' due to lowering θ as a consequence of Si–N → Al–O replacement) and defect concentration (increase of the intercept B' due to Al on Si site and O on N site acting as scattering centres for phonons) (Fig. 7 and Table 3).

A problem in the comparison of the different samples is that they often show a considerable anisotropy; in particular all recently produced samples with conductivities $>100\,W\,m^{-1}\,K^{-1}$ have elongated grains. The anisotropy was clearly demonstrated by Li et al. using thermoreflectance microscopy to measure the conductivity inside individual grains[54]. They found conductivity-values of $69\,W\,m^{-1}\,K^{-1}$ along the a-axis and $180\,W\,m^{-1}\,K^{-1}$ along the c-axis. The consequences of anisotropy for the a^{-1} versus T plot are clearly visible in Fig. 8 for a tape-cast sample. This plot shows two different slope values, the one in the casting direction (predominantly along c-axis) below the typically observed value and the one in the stacking direction (predominantly along a-axis) above the typically observed slope value (Table 3).

5. Discussion

From the results of the a^{-1} versus T plots it is clear that these plots can be very useful for optimisation of the thermal diffusivity. The data of a material processed in different ways can be used to study the influence of different additives. Increase of the slope indicates that the additive dissolves into the lattice, whereas a decrease in slope or intercept indicates that the additive improves the thermal conductivity.

5.1. Interpretation of the fitting parameters

In general the observed slopes A' for the three materials have a typical constant value ($MgSiN_2$: 400–430 $m^{-2}\,s\,K^{-1}$ (Table 1); AlN: 80–90 $m^{-2}\,s\,K^{-1}$ (Table 2); and β-Si_3N_4: 100–130 $m^{-2}\,s\,K^{-1}$ (Table 3)) and deviations from this constant value can be explained in view of the lattice characteristics. For the samples with the same lattice characteristics (constant A') but with different impurity content and microstructure a relatively large variation in the intercept value B' can be observed. Considering the large variation in thermal conductivity observed for the samples with an approximately constant slope, it can be concluded that all phonon scattering processes, except the intrinsic phonon-phonon scattering, are indeed (almost) temperature independent. As expected from the theory, also negative intercept values are found. Furthermore AlN with the lowest slope value A' shows the highest reduced Debye temperature $\tilde{\theta}_0$ (Table 4). This indicates that the presented theoretical concept has a sound basis.

5.2. Thermal conductivity estimates for $MgSiN_2$, AlN and β-Si_3N_4

In order to estimate the maximum achievable theoretical thermal diffusivity ($B = 0$), besides the slope A' the intercept with the a^{-1}-axis or the T-axis should be known. For the present discussion the intercept with the T-axis was used as this value is only dependent on $\tilde{\theta}$ and b.

5.2.1. Determination of θ and b

Assuming that the acoustic phonons are the major heat carriers, the high temperature limit of the Debye temperature based on the acoustic phonons θ_∞^A is needed[10] to evaluate the reduced Debye temperature $\tilde{\theta}$. Since θ_∞^A is often not available it is normally approximated by the Debye temperature evaluated from elastic constants or heat capacity data near 0 K[10,30,55] resulting in θ_0. Therefore θ_0 data for $MgSiN_2$, AlN and Si_3N_4[55] obtained from elastic constants

Table 4
The measured slope A' ($= bA/\tilde{\theta}$), the Debye temperature θ, the number of atoms per primitive unit cell n, the resulting reduced Debye temperature $\tilde{\theta}$ ($=\theta/n^{1/3}$) and the calculated intercept ($=\tilde{\theta}/2b$ with $b = 2$) for $MgSiN_2$, AlN and β-Si_3N_4

Material	Slope A' ($m^{-2}\,s\,K^{-1}$)	θ (K)	n	$\tilde{\theta}$ (K)	Intercept (b=2) (K)
$MgSiN_2$	400–430	900[55]	16[63]	357	89
AlN	80–90	940[55]	4[57]	592	148
β-Si_3N_4	100–130	955[55]	14[64]	396	99
		1156[56]		480	120

Data from Ref. 55 are for θ_0, data from Ref. 56 are for θ^A.

were used to calculate $\tilde{\theta}$ (Table 4). The number of atoms per primitive unit cell n can be obtained from crystallographic data (Table 4). This results in reduced Debye temperatures ($\tilde{\theta}_0$) of 357, 592 and 396 K for $MgSiN_2$, AlN and Si_3N_4, respectively. For Si_3N_4 Morelli and Heremans[56] recently calculated $\tilde{\theta}^A_\infty = 480$ K. As shown in Table 5, the use of $\tilde{\theta}_0 = 396$ K instead of 480 K for Si_3N_4 leads to a 10% lower conductivity at 300 K and only 3% at 600 K.

The value of b for describing the temperature dependence of the thermal diffusivity is not exactly known. Based on the simple Debye theory it can be argued that $b = 2$[16,17,23,25]. However, b may differ somewhat from 2 and vary from substance to substance[16]. Leibfried and Schlömann[19] suggest that for a FCC lattice $b = \sqrt{5}/3 = 1.29$. However, the scarce experimental results confirm the value of $b \approx 2$ (2.3, 2.7 and 2.1 for solid helium, diamond and sapphire, respectively[17]). Taking $b = 2$ results in theoretically calculated intercepts of 89, 148 and 99 K for pure, defect free $MgSiN_2$, AlN and Si_3N_4 ceramics, respectively (Table 4).

5.2.2. Comparison between theoretical and experimental intercept with the T-axis

The theoretical intercept with the T-axis of $MgSiN_2$ is as expected higher than the experimentally observed value. However, for β-Si_3N_4 and AlN, particularly for the anisotropic samples, this is not always the case. Moreover, for AlN phonon dispersion curves indicate that also optic phonons contribute to the heat conduction resulting in an underestimation of the reduced Debye temperature[57]. When using the a^{-1} versus T method, both the slope A' and the (theoretical) intercept with the T-axis are related to $\tilde{\theta}$. However, especially at high temperatures the influence of $\tilde{\theta}$ on the estimate is limited as $a^{-1} = A'T + B' \approx A'T$ and A' is determined experimentally (see Table 5: 600 and 900 K estimates). This makes the estimates for the thermal diffusivity less sensitive for errors induced by not taking optic phonons fully into account.

5.2.3. Thermal conductivity estimates

Using the data in Table 4, together with available values of the density and heat capacity, we can estimate the intrinsic thermal conductivity (see Eq. (1)) at temperatures $T \geq \tilde{\theta}/2$ ($T \geq 179$, 296 and 198 K for $MgSiN_2$, AlN and β-Si_3N_4, respectively). Results at 300, 600 and 900 K are shown in Table 5, together with experimentally obtained values. For these calculations we used the lowest values of the slope since we want to estimate the maximum diffusivity. This is still a conservative estimate since the Debye temperature used in our calculation may be too low due to neglect of optical phonon contributions.

For $MgSiN_2$ ceramics the highest experimentally obtained thermal conductivity at 300 K (Table 5) does not

Table 5
The estimates for the maximum achievable thermal conductivity κ_{the} at 300, 600 and 900 K, using the data of Table 4 for $MgSiN_2$, AlN and β-Si_3N_4 together with the molar density ρ_m and heat capacity C_p, compared with corresponding highest experimentally observed thermal conductivity κ_{exp}

Material	a ($m^2\,s^{-1}$)	ρ_m ($mol\,m^{-3}$)	$C_p = C_V$ ($J\,mol^{-1}\,K^{-1}$)	κ_{the} ($W\,m^{-1}\,K^{-1}$)	κ_{exp} ($W\,m^{-1}\,K^{-1}$)
300 K					
$MgSiN_2$	1.18×10^{-5}	3.90×10^4	61.7	28	23
AlN	8.22×10^{-5}	7.94×10^4	30.6	200	246–266
β-Si_3N_4	4.52×10^{-5}	2.29×10^4	90.6	94	107
	5.05×10^{-5}			105	
600 K					
$MgSiN_2$	0.49×10^{-5}	3.88×10^4	88.1	17	15
AlN	2.77×10^{-5}	7.91×10^4	44.0	96	96
β-Si_3N_4	1.81×10^{-5}	2.28×10^4	144.5	60	76
	1.89×10^{-5}			62	
900 K					
$MgSiN_2$	0.31×10^{-5}	3.86×10^4	95.6	11	11
AlN	1.66×10^{-5}	7.87×10^4	47.7	62	55
β-Si_3N_4	1.13×10^{-5}	2.27×10^4	157.0	40	45
	1.17×10^{-5}			42	

exceed $25\,W\,m^{-1}\,K^{-1}$ despite the fact that already considerable effort has been made to improve the thermal conductivity[9,33,34,55,58,59]. As the predicted value of $28\,W\,m^{-1}\,K^{-1}$ is close to this value, it can be concluded that the highest experimentally observed value is close to the intrinsic one. From Tables 1 and 5 and Fig. 2 it is obvious that a further reduction of the defect concentration in the $MgSiN_2$ lattice will not result in a significant increase of the thermal diffusivity, because for the best samples the intercept with the *T*-axis of 45 K (Table 1 and Fig. 2) is already very close to the theoretical value of 89 K (Table 4).

For AlN the highest experimental value for a ceramic sample is $266\,W\,m^{-1}\,K^{-1}$[60], higher than our estimate of about $200\,W\,m^{-1}\,K^{-1}$. A problem with the comparison of the experimental value is that optimisation of the microstructure leads to anisotropic grains and therefore higher values than can be expected from our calculations since we then underestimate the intercept with the *T*-axis (see Section 5.2.2). For the estimates at 600 and 900 K the agreement between estimated and experimental values improves as the exact value of the intercept with the *T*-axis is of less importance as $a^{-1} = A'T + B' \approx A'T$ (at high temperature). The value of $319\,W\,m^{-1}\,K^{-1}$ reported in Ref. 40 is based on extrapolation of the single crystal data obtained for the *c*-axis and therefore cannot be compared to our isotropic value. Our estimation also agrees better with the experimental data than the value calculated from the Slack formula (Table 6), which is more sensitive for errors in the reduced Debye temperature.

The estimates for β-Si_3N_4 at 300, 600 and 900 K are close to the experimentally observed values (Table 5), but as mentioned earlier room temperature values higher than $100\,W\,m^{-1}\,K^{-1}$ are all obtained on anisotropic samples. From the conductivity data measured along the *a*- and *c*-axes in a single grain[54], one can estimate an average isotropic value of about $106\,W\,m^{-1}\,K^{-1}$, close to our estimation of $105\,W\,m^{-1}\,K^{-1}$.

In general the theoretical estimates are in good agreement (within 20%) with the best experimentally observed values (Table 5). If the intercept with the *T*-axis is underestimated (like in the case of AlN due to optic phonons contributing substantially to the heat conduction) the maximum achievable thermal conductivity is underestimated. However, at higher temperatures ($T > 3 \times (1/4)\tilde{\theta}_0$) the exact value of the intercept with the *T*-axis becomes less important. At high temperatures the accuracy of the estimate is consequently determined by the error in the slope A'. As for most applications the thermal conductivity at elevated temperature (>300 K) is of importance, the estimate of the intercept is considered sufficiently accurate.

5.3. Limitations, accuracy and reliability

It should be noted that the new estimation method based on Eq. (5) was obtained by approximating an already simple description of the (temperature dependence of the) thermal diffusivity (Eq. (4)) of a pure phonon conductor. Furthermore the values of $b = 2$ and θ used to calculate the intercept with the *T*-axis are somewhat arbitrary. For practical use the choice of $b = 2$ and $\theta = \theta_0$ seems to work out reasonably well as θ_0 can be easily obtained from elastic constants and reasonable, somewhat conservative, estimates for the

Table 6
Estimates of the thermal conductivity for $MgSiN_2$, AlN and β-Si_3N_4 ceramics at 300 K, based on different theoretical approximations

	Estimated value ($W\,m^{-1}\,K^{-1}$)	Reference	Estimation method based on
	$MgSiN_2$	14	$\kappa_{exp} = 23\,W\,m^{-1}\,K^{-1}$
	28	This work	a^{-1} vs. T
	34	65	Standard Slack equation
	26 ± 4	14	Thermal diffusivity measurements
	35–50	58	Defect scattering
	40–70	58	Slack equation
	75	66	Slack equation
Time↑	120	8	Not specified*
	AlN		$\kappa_{exp} = 266\,W\,m^{-1}\,K^{-1}$[60]
	200	This work	a^{-1} vs. T
	128	65	Slack equation
	319**	40	Defect scattering
Time↑	320	2	Scaling factor $M\delta\theta^3$
	β-Si_3N_4		$\kappa_{exp} = 106\,W\,m^{-1}\,K^{-1}$[54]
	105	This work	a^{-1} vs. T
	260	67	Molecular dynamics
	250	56	Slack formula
	124	65	Slack formula
	177**	7	Two-phase composite model
Time↑	200–320	5	Slack equation

For comparison the highest measured values (κ_{exp}) are also given (*probably based on $n^{-2/3}$ dependence of the Slack equation[10] and the estimate of the intrinsic thermal conductivity of about $300\,W\,m^{-1}\,K^{-1}$ for AlN; **anisotropic values).

theoretical thermal conductivity are obtained. As shown for Si_3N_4 even better agreement is obtained if values for the $\tilde{\theta}_{\infty}^{A}$ are available.

The presented estimation method seems to be more reliable than the theoretical Slack equation[10] (Table 6). This can be explained in view of the influence of the accuracy of the reduced Debye temperature on the resulting estimate. The (more complicated) Slack equation is very sensitive for relatively small deviations in the input parameters, whereas the here presented method is relatively easy applicable and less sensitive for small deviations in slope and intercept. In general, the Slack equation is especially useful when no samples for thermal diffusivity measurements are available, whereas the a^{-1} versus T plots give a more accurate indication of the maximum achievable thermal conductivity and additionally can be used to guide processing optimisation in order to obtain the desired thermal conductivity.

6. Conclusions

A new, simple method for estimating the achievable (intrinsic) thermal conductivity of non-metallic compounds was presented, based on temperature dependent thermal diffusivity measurements. Its strength is that non-optimised samples can be used to provide a good impression of the intrinsic thermal conductivity. It was successfully applied to $MgSiN_2$, AlN and β-Si_3N_4 providing some evidence for its general applicability. For AlN at 300 K a too low estimate was obtained due to the fact that the intercept with the T-axis was underestimated as optic phonons, which are not considered, contribute substantially to the heat conduction. In general the estimates are accurate within 20% and become more accurate with increasing temperature, independent of the fact whether or not optic phonons contribute substantially to the heat conduction. Furthermore, the method is a useful tool for optimising the processing as it enables discrimination between the lattice characteristics, defects and microstructure.

Acknowledgements

The authors would like to thank Dr. R. Bogaard (Purdue University) for providing the raw data of Refs. 31,41, Dr. K. Watari (National Industrial Research Institute of Nagoya (NIRIN), Nagoya, Japan) for providing some of the data for (β-)Si_3N_4, Dr. N. Hirosaki (National Institute for Research in Inorganic Materials (NIRIM), Japan) for providing the data of Ref. 50, Dr. H.J. Sölter (CompoTherm Messtechnik GmbH, Germany) for measuring the thermal diffusivity of the $MgSiN_2$ samples and Professor Dr. G. de With (Eindhoven University of Technology, The Netherlands) for reading and commenting on the manuscript.

References

1. Roosen, A., *Modern Substrate Concepts for the Microelectronic Industry, Electroceramics IV 2, Aachen (Germany), September 5–7, 1994*, ed. R. Waser, S. Hoffmann, D. Bonnenberg and Ch. Hoffmann. Augustinus Buchhandlung, 1994, p. 1089.
2. Borom, M. P., Slack, G. A. and Szymaszek, J. W., Thermal conductivity of commercial aluminum nitride. *Bull. Am. Ceram. Soc.* 1972, **51**, 852.
3. Werdecker, W. and Aldinger, F., Aluminum nitride—an alternative ceramic substrate for high power applications in microcircuits. *IEEE Trans. Compon. Hybrids Manuf. Technol.* 1984, **CHMT-7**, 399–404.
4. Jackson, T. B., Virkar, A. V., More, K. L., Dinwiddie, Jr. R.B. and Cutler, R. A., High-thermal-conductivity aluminum nitride ceramics: the effect of thermodynamic, kinetic, and microstructural factors. *J. Am. Ceram. Soc.* 1997, **80**, 1421.
5. Haggerty, J. S. and Lightfoot, A., Opportunities for enhancing the thermal conductivities of SiC and Si_3N_4 ceramics through improved processing. In *Ceram. Eng. Sci. Proc. 16, 19th Annual Conference on Composites, Advanced Ceramics, Materials, and Structures-A, Cocoa Beach, Florida, USA, January 8–12, 1995*, ed. J. B. Wachtman. The American Ceramic Society, Westerville, OH, 1995, p. 475.
6. Watari, K., Hirao, K., Brito, M. E., Toriyama, M. and Kanzaki, S., Hot isostatic pressing to increase thermal conductivity of Si_3N_4 ceramics. *J. Mater. Res.* 1999, **14**, 1538.
7. Hirao, K., Watari, K., Brito, M. E., Toriyama, M. and Kanzaki, S., High thermal conductivity of silicon nitride with anisotropic microstructure. *J. Am. Ceram. Soc.* 1996, **79**, 2485.
8. Groen, W. A., Kraan, M. J., de With, G. and Viegers, M. P. A., New covalent ceramics: $MgSiN_2$. In *Mater. Res. Soc. Symp., Vol 327, Covalent Ceramics. II. Non-Oxides, Boston, OH, USA, November 1993*, ed. A. R. Barron, G. S. Fischman, M. A. Fury and A. F. Hepp. Materials Research Society, Pittsburgh, 1994, p. 239.
9. Davies, I. J., Shimazaki, T., Aizawa, M., Suemasu, H., Nozue, A. and Itatani, K., Physical properties of hot-pressed magnesium silicon nitride compacts with yttrium oxide addition. *Inorg. Mater.* 1999, **6**, 276.
10. Slack, G. A., *The Thermal Conductivity of Nonmetallic Crystals, Solid State Physics, Vol 34*, ed. F. Seitz, D. Turnbull, H. Ehrenreich. Academic Press, New York, 1979, p. 1.
11. Chavat, F. R. and Kingery, W. D., Thermal conductivity. XIII. Effect of microstructure on conductivity of single-phase ceramics. *J. Am. Ceram. Soc.* 1957, **40**, 306.
12. Liu, D.-M. and Lin, B.-W., Thermal conductivity in hot-pressed silicon carbide. *Ceram. Int.* 1996, **22**, 407.
13. Kingery, W. D., Thermal conductivity. XII. Temperature dependence of conductivity for single-phase ceramics. *J. Am. Ceram. Soc.* 1955, **38**, 251.
14. Bruls, R. J., Hintzen, H. T. and Metselaar, R., Modeling of the thermal diffusivity/conductivity of $MgSiN_2$ ceramics, ITCC 24 and ITES 12. In *24th International Thermal Conductivity Conference and 12th International Thermal Expansion Symposium, Pittsburgh, PA, USA, October 26–29, 1997*, ed. P. S. Gaal and D. E. Apostolescu. Technomic Publishing Co., Inc., Lancaster, 1999, p. 3.
15. Berman, R., *Thermal Conduction in Solids*. Clarendon Press, Oxford, 1976.
16. Debye, P., Zustandsgleichung und Quantenhypotheses mit einem Anhang über Wärmeleitung. In *Vorträge über die Kinetische Theorie der Materie und der Elektrizität*. Teubner, Berlin, 1914, pp. 19–60.
17. Berman, R., The thermal conductivity of dielectric solids at low temperatures. *Adv. Phys.* 1953, **2**, 103.
18. Klemens, P. G., *Theory of the Thermal Conductivity of Solids, Thermal Conductivity, Vol 1*, ed. R. P. Tye. Academic Press, London, 1969.
19. Leibfried, G. and Schlömann, E., Wärmeleitung in elektrisch isolierenden Kristallen. *Nachr. Akad. Wiss. Göttingen, Math. Physik. Kl* 1954, **IIa**, 71.

20. Klemens, P. G., Thermal conductivity of dielectric solids at low temperatures. *Proc. R. Soc. Lond.* 1951, **A208**, 108.
21. Klemens, P. G., *Thermal Conductivity and Lattice Vibrational Modes, Solid State Physics, Vol 7*, ed. F. Seitz and D. Turnbull. Academic Press Inc., New York, 1958, p. 1.
22. Watari, K., Ishazaki, K. and Tsuchiya, F., Phonon scattering and thermal conduction mechanisms of sintered aluminium nitride ceramics. *J. Mater. Sci.* 1993, **28**, 3709.
23. Peierls, R., Zur kinetischen Theorie der Wärmeleitung in Kristallen. *Ann. Phys.* 1929, **3**, 1055.
24. Roufosse, M. and Klemens, P. G., Thermal conductivity of complex dielectric crystals. *Phys. Rev. B* 1973, **7**, 5379.
25. Drabble, J. R. and Goldsmid, H. J., *International Series of Monographs on Semiconductors, Vol 4: Thermal Conduction in Semiconductors*, ed. H. K. Henisch. Pergamon Press, Oxford, 1961, p. 141.
26. Collins, A. K., Pickering, M. A. and Taylor, R. L., Grain size dependence of the thermal conductivity of polycrystalline chemical vapor deposited β-SiC at low temperatures. *J. Appl. Phys.* 1990, **68**, 6510.
27. Klemens, P. G., Thermal resistance due to point defects at high temperatures. *Phys. Rev.* 1960, **119**, 507.
28. Ambegaokar, V., Thermal resistance due to isotopes at high temperatures. *Phys. Rev.* 1959, **114**, 488.
29. Klemens, P. G., *Thermal Conductivity of Lattice Vibrational Modes, Solid State Physics, Vol 7*, ed. F. Seitz and D. Turnbull. Academic Press Inc., Publishers, New York, 1958, p. 1.
30. Debije, P., Zur Theorie der spezifischen Wärmen. *Ann. Physik* 1912, **39**, 789.
31. Enck, R. C. and Harris, R. D., Temperature dependence of thermal conductivity of electronic ceramics by an improved flash diffusivity technique. In *Mater. Res. Soc. Proc., Vol 167, Advanced Electronic Packaging Materials, Boston, Massachusetts, USA, November 27–29, 1989*, ed. A. T. Barfknecht, J. P. Partridge, C. J. Chen and C.-Y. Li. Materials Research Society, Pittsburgh, 1990, p. 235.
32. Roufosse, M. C. and Klemens, P. G., Lattice thermal conductivity of minerals at high temperatures. *J. Geophys. Res.* 1974, **79**, 703.
33. Hintzen, H. T., Bruls, R., Kudyba, A., Groen, W. A. and Metselaar, R., Powder preparation and densification of $MgSiN_2$. In *Ceram. Trans. 51 Int. Conf. Cer. Proc. Sci. Techn., Friedrichshafen, Germany, September 1994*, ed. H. Hausner, G. L. Messing, S. Hirano. The American Ceramic Society, 1995, p. 585.
34. Hintzen, H. T., Swaanen, P., Metselaar, R., Groen, W. A. and Kraan, M. J., Hot-pressing of $MgSiN_2$ ceramics. *J. Mater. Sci. Lett.* 1994, **13**, 1314.
35. Bruls, R. J., Kudyba-Jansen, A. A., Gerharts, P., Hintzen, H. T. and Metselaar, R., Preparation, characterisation and properties of $MgSiN_2$ ceramics. *J. Mater. Sci. Mater. Electr.* 2002, **13**, 63.
36. Parker, W. J., Jenkins, R. J., Butler, C. P. and Abbott, G. L., Flash method of determining thermal diffusivity, heat capacity, and thermal conductivity. *J. Appl. Phys.* 1961, **32**, 1679.
37. Bruls, R. J., Hintzen, H. T., de With, G., Metselaar, R. and van Miltenburg, J. C., The temperature dependence of the Grüneisen parameter of $MgSiN_2$, AlN and β-Si_3N_4. *J. Phys. Chem. Solids* 2001, **62**, 783.
38. Bruls, R. J., Hintzen, H. T., Metselaar, R. and van Miltenburg, J. C., Heat capacity of $MgSiN_2$ between 8 and 800 K. *J. Phys. Chem. B* 1998, **102**, 7871.
39. Swalin, R. A., *Thermodynamics of Solids* (*2nd ed.*). Wiley, New York, 1972, p. 82.
40. Slack, G. A., Tanzilli, R. A., Pohl, R. O. and Vandersande, J. W., The intrinsic thermal conductivity of AlN. *J. Phys. Chem. Solids* 1987, **48**, 641.
41. Rohde, M. and Schulz, B., Thermal conductivity of irradiated and non-irradiated fusion ceramics. In *21st International Thermal Conductivity Conference and 9th International Thermal Expansion Symposium (ITCC 21 and ITES 9), 1990*, ed. C. J. Cremers and H. A. Fine. Plenum Publishing, New York, 1990, p. 509.
42. Jackson, T. B., Donaldson, K. Y. and Hasselman, D. P. H., Temperature dependence of the thermal diffusivity/conductivity of aluminum nitride. *J. Am. Ceram. Soc.* 1990, **73**, 2511.
43. de Baranda, P. S., *Thermal Conductivity of Aluminum Nitride*. Ph.D. Thesis, Rutgers University, Piscataway, NJ, USA, 1991, pp. 1–294.
44. de Baranda, P. S., Knudsen, A. K. and Ruh, E., Effect of CaO on the thermal conductivity of aluminum nitride. *J. Am. Ceram. Soc.* 1993, **76**, 1751.
45. de Baranda, P. S., Knudsen, A. K. and Ruh, E., Effect of silica on the thermal conductivity of aluminum nitride. *J. Am. Ceram. Soc.* 1993, **76**, 1761.
46. Witek, A., Bockowski, M., Presz, A., Wróblewski, M., Krukowski, S., Wlosinski, W. and Jablonski, K., Synthesis of oxygen-free aluminum nitride ceramics. *J. Mater. Sci.* 1998, **33**, 3321.
47. Tsukuma, K., Shimada, M. and Koizumi, M., Thermal conductivity and microhardness of Si_3N_4 with and without additives. *Am. Ceram. Soc. Bull.* 1981, **60**, 910.
48. Watari, K., Seki, Y. and Ishizaki, K., Temperature dependence of thermal coefficients for HIPped sintered silicon nitride. *J. Ceram. Soc. Jpn. Int. Ed.* 1989, **97**, 170.
49. Peletskii, V. E., The investigation of thermal conductivity of silicon nitride. *High Temp.*, 1993, **31**, 668 [translated from *Teplofizika Vysokikh Temperatur.*, 1993, **31**, 727].
50. Hirosaki, N., Okamoto, Y., Ando, M., Munakata, F. and Akimunde, Y., Effect of grain growth on the thermal conductivity of silicon nitride. *J. Ceram. Soc. Jpn. Int. Ed.* 1996, **104**, 50.
51. Watari, K., Brito, M. E., Toriyama, M., Ishizaki, K., Cao, S. and Mori, K., Thermal conductivity of Y_2O_3-doped Si_3N_4 ceramics at 4 to 1000 K. *J. Mater. Sci. Lett.* 1999, **18**, 865.
52. Virkar, A. V., Jackson, T. B. and Cutler, R. A., Thermodynamic and kinetic effects of oxygen removal on the thermal conductivity of aluminum nitride. *J. Am. Ceram. Soc.* 1989, **72**, 2031.
53. Buhr, H., Müller, G., Wiggers, H., Aldinger, F., Foley, P. and Roosen, A., Phase composition, oxygen content, and thermal conductivity of $AlN(Y_2O_3)$ ceramics. *J. Am. Ceram. Soc.* 1991, **74**, 718.
54. Li, B., Pottier, L., Roger, J. P., Fournier, D., Watari, K. and Hirao, K., Measuring the anisotropic thermal diffusivity of silicon nitride grains by thermoreflectance microscopy. *J. Eur. Ceram. Soc.* 1999, **19**, 1631.
55. Bruls, R. J., Hintzen, H. T., de With, G. and Metselaar, R., The temperature dependence of the Young's modulus of $MgSiN_2$, AlN and Si_3N_4. *J. Eur. Ceram. Soc.* 2001, **21**, 263.
56. Morelli, D. T. and Heremans, J. P., Thermal conductivity of germanium. *Appl. Phys. Lett.* 2002, **81**, 5126.
57. Nipko, J. C. and Loong, C.-K., Phonon excitations and related thermal properties of aluminium nitride. *Phys. Rev. B* 1998, **57**, 10550.
58. Hintzen, H. T., Bruls, R. J. and Metselaar, R., Thermal conductivity of $MgSiN_2$ ceramics. In *Fourth Euroceramics 2, Faenza (Italy), October 1995*, ed. C. Galassi. Gruppo editoriale Faenza editrice S.p.A., Faenza, 1995, p. 289.
59. Davies, I. J., Uchida, H., Aizawa, M. and Itatani, K., Physical and mechanical properties of sintered magnesium silicon nitride compacts with yttrium oxide addition. *Inorg. Mater.* 1999, **6**, 40.
60. Okamoto, M., Arakawa, H., Oohashi, M. and Ogihara, S., Effect of microstructure on thermal conductivity of AlN ceramics. *J. Ceram. Soc. Jpn. Int. Ed.* 1989, **97**, 1486.
61. Slack, G. A. and McNelly, T. F., AlN single crystals. *J. Crystal Growth* 1977, **42**, 560.
62. Bogaard, R. H., personal communication, providing the raw data for Refs. 31,41.
63. David, J., Laurent, Y. and Lang, J., Structure de $MgSiN_2$ et $MgGeN_2$. *Bull. Soc. Fr. Minéral. Cristallogr.* 1970, **93**, 153.
64. Grün, R., The crystal structure of β-Si_3N_4; structural and stability considerations between α- and β-Si_3N_4. *Acta Crystallogr.* 1979, **B35**, 800.
65. Bruls, R. J., *The Thermal Conductivity of Magnesium Silicon Nitride Ceramics and Related Materials*. Ph.D. Thesis, Eindhoven University of Technology, University Press TU Eindhoven, 2000, Chapter 8.

66. de With, G. and Groen, W. A., Thermal conductivity estimates for new (oxy)-nitride ceramics. In *Fourth Euroceramics 3, Faenza (Italy), October 1995*, ed. S. Meriani and V. Sergo. Gruppo editoriale Faenza editrice S.p.A., Faenza, 1995, p. 405.

67. Hirosaki, N., Ogata, S., Kocer, C., Kitagawa, H. and Nakamura, Y., Molecular dynamics calculation of the ideal thermal conductivity of single-crystal α- and β-Si_3N_4. *Phys. Rev.* 2002, **B65**, 134110.